Flow of a falling liquid curtain onto a moving substrate

Flow of a falling liquid curtain onto a moving substrate

Flow of a falling liquid curtain onto a moving substrate

Flow of a Falling Liquid Curtain onto a Moving Substrate

Yekun Liu[1], Masahiro Itoh[1], and Harumichi Kyotoh[2]

[1]Graduate school of Engineering Mechanics and Systems, University of Tsukuba, Tsukuba, Ibaraki 302-8573, Japan

[2]Division of Engineering Mechanics and Systems, University of Tsukuba, Tsukuba, Ibaraki 302-8573, Japan

E-mail: yekunliu@hotmail.com

Abstract. In this study, we investigate a low-Weber-number flow of a liquid curtain bridged between two vertical edge guides and the upper surface of a moving substrate. Surface waves are observed on the liquid curtain, which are generated due to a large pressure difference between the inner and outer region of the meniscus on the substrate, and propagate upstream. They are categorised as varicose waves that propagate upstream on the curtain and become stationary because of the downstream flow. The Kistler's equation, which governs the flow in thin liquid curtains, is solved under the downstream boundary conditions, and the numerical solutions are studied carefully. The solutions are categorised into three cases depending on the boundary conditions. The stability of the varicose waves is also discussed as wavelets were observed on these waves. The two types of modes staggered and peak-valley patterns are considered in the present study, and they depend on the Reynolds number, the Weber number, and the amplitude of the surface waves. The former is observed in our experiment, while the latter is predicted by our calculation. Both the types of modes can be derived using the equations with periodic coefficients that originated from the periodic base flow due to the varicose waves. The stability analysis of the waves shows that the appearance of the peak-valley pattern requires a significantly greater amplitude of the waves, and a significantly higher Weber number and Reynolds number compared to the condition in which the staggered pattern is observed.

1. Introduction

Coating of a thin liquid layer on numerous high quality products is an important step in industrial manufacturing [1]. The process of coating involves overlaying one or several liquid layers onto the surface of products. After this process, the thin liquid layers are ultimately transformed into a solid coat that offers specific functions for products via chilling, drying, or some other means [2].

In recent years, miniaturised and high precision liquid-crystal display (LCD) screens, which are used for small displays have been rapidly developed. The thin and high-precision film covering the LCD screen is manufactured by a slide coating method, in which the coating layer can be influenced by the oscillation of the slot and the substrate, as the distance between them is considerably small. On the other hand, curtain coating can avoid this type of influence, and is a good method for coating on rugged substrates. However, curtain coating has not been applied to LCD screens, because the liquid curtain with small discharge, i.e. small Weber number, causes instabilities of the flow and the free surfaces [3].

1

As a new coating method, curtain coating has two outstanding advantages—it can coat extremely thin layers on irregular surfaces and this process can be carried out with rather high coating speeds. The difficulties involved with this method are mostly related to the freely falling liquid curtain. One of the difficulty is that the liquid curtain breaks up easily once the flow rate is under a threshold [4]. The other difficulty is the susceptibility to the disturbance of the freely falling liquid curtain, leading to unevenness of the coating layer. Given the two difficulties, this method is mostly applied with a high Weber number, i.e. $We > 2$, which implies that the inertial force is larger than the surface tension. We is defined by $\rho q U / \gamma$ where ρ, q, U and γ denote the liquid density, the unit discharge, the liquid velocity and the surface tension, respectively. New possibilities in curtain coating have been explored by examining the flow of a freely falling liquid curtain with a low Weber number ($We < 2$) [5]. Nevertheless, it focuses on the flow of the liquid curtain into a pool and not a substrate. In our study, we focus on a freely falling liquid curtain onto a substrate with a rather low Weber number ($We < 0.2$), and a roller and a conveyer belt are employed as the substrate. The discharge of the liquid is quite small, below which the liquid curtain does not form. In this case, the flow of the liquid curtain is significantly influenced by the surface tension and not the inertial force.

One of the serious problems in curtain coating is the instability of the liquid film [6]. The influence of gravity and applied pressure of the surrounding air is important for the stability of the liquid curtain, which can clearly affect the curtain shape [7]. The wetting process [8-10], besides affecting the air entrainment [11], can also influence the patterns of the liquid curtain. Higher viscosity, which can enhance the critical speed at which the air entrainment occurs, is a good way to avoid dynamic wetting failure [12]. In fact, higher viscosity can also affect the stability of the liquid curtain [3]. Besides, the effects of surface tension on a liquid sheet falling in the gravitational field is also important [13].

A number of important works on the stability of falling liquid curtain have been overlooked. Lin examined the stability of a viscous liquid curtain falling down steadily under the influence of gravity [14]. Li and Tankin investigated the temporal stability of a two-dimensional viscous liquid sheet [15]. Li focused on the spatial stability of a thin moving viscous plane liquid sheet in a resting inviscid gas medium [16]. Benilov *et al.* conducted a research on the stability of thin liquid curtain with respect to two-dimensional perturbations [17]. Liu *et al.* analysed the weakly nonlinear stability of a viscous planar liquid sheet moving in an inviscid stationary gas ambience by a perturbation expansion technique [18].

In the present study, we have considered a curtain coating wherein the height of the curtain is comparable to the meniscus formed above the substrate. The Weber number in the present study is quite low; therefore, the curtain is formed because of the bridging between the die exit and the roller surface. On the other hand, we have observed large amplitude varicose waves. In this study, we observe the variation in these waves under different conditions, and find a suitable environmental condition for the coating process.

The contents of the present study are as follows. Section 2 introduces the experimental method and the experimental results with various experimental conditions of liquids, falling heights, substrate speeds, and process of pre-wetting. Section 3 shows the equations governing the liquid curtain profile, their approximate solutions, the numerical analysis and the analysis of the stability of the liquid curtain. Finally, in section 4, our studies are summarized.

2. Experimental Analysis

2.1. Experimental set-up

Figure 1 shows the experimental setup used in the present study. Liquid is circulated from a tank to a slot using a pump (ORIENTAL MOTOR Usm540-401W). The slot die has a width of 60 mm. Two vertical edge guides are installed on both sides of the slot, and a liquid curtain forms a bridge between these guides. The edge guides, each having a diameter of 1 mm, are composed of stainless steel. In order to understand the effect of different shapes' substrate to the profiles of liquid curtains, two types of substrates—roller and conveyer belt—are used in our experiment, both of which are made up of stainless steel. The roller has a diameter of 37 mm and a width of 60 mm, while the conveyer belt has a length of 500 mm and a width of 60 mm.

(a)   (b)
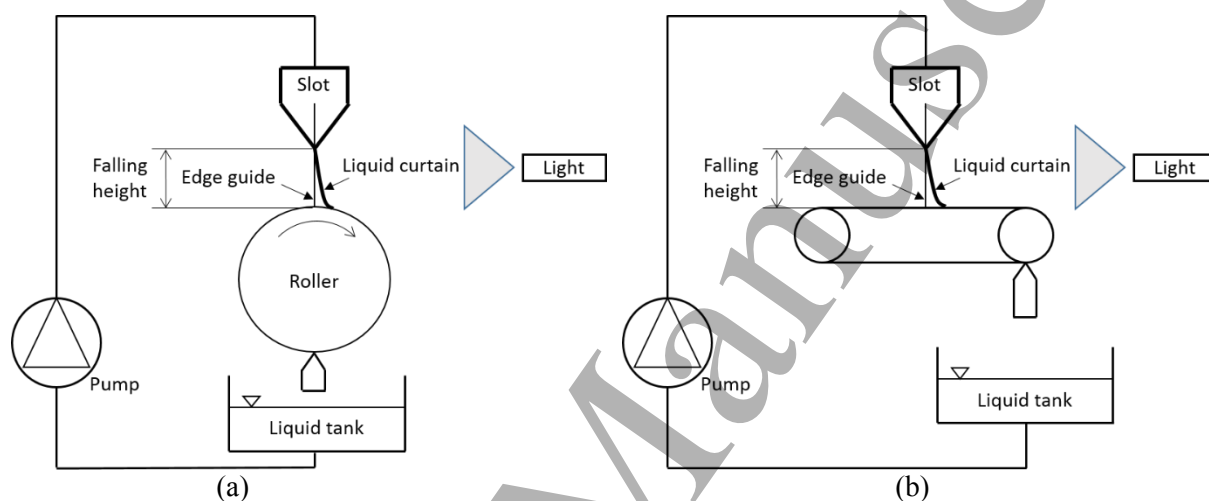
Figure 1. Experimental setup with different substrates. (a) Roller (b) Conveyer belt
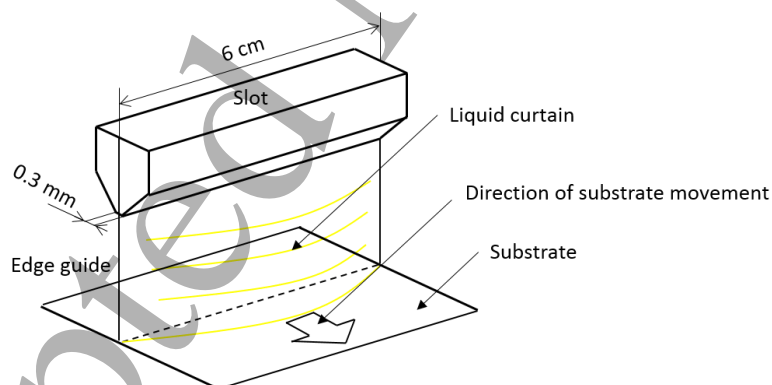
Figure 2. Flow visualization.

The curtain thus forms between the exit of the slot and the upper surface of the substrate. As shown in figure 2, the curtain pattern is visualized by the lamp (M-Visual Light Source LD-M210) over the liquid curtain, and images and videos are obtained by a high-speed camera (Photron Fastcam SA4).

2.2. Surface waves

Surface waves are observed for all the cases investigated in this study. As the substrate speed is rather low compared to the velocity of the liquid curtain, the curtain profile is nearly vertical and the flow of curtain vertically impinges on the substrate surface. The meniscus develops from the curtain to the roller's surface. As the Weber number is very small, i.e. the inertial force is much lesser than the surface tension and the pressure difference between the inner and outer region of the meniscus on the surface of

3

the substrate is considerably large, surface waves are produced and develops upstream as shown in figure 3. In the present paper, We_{sub}, Ca_{sub}, Re denote the Weber number above the substrate, the Capillary number above the substrate, and the Reynolds number, and are defined by $\rho q U_s / \gamma$, $\mu U_s / \gamma$, and $\rho q / \mu$, respectively. Here, ρ, q, U_s, γ, and μ denote the liquid density, the unit discharge, the liquid velocity at the bottom of the liquid curtain, the surface tension, and the viscosity, respectively. The captions of parameters in the experiments appearing in figure 4, 6, 8 and 9 are listed in table 1. We established that the wave number and the wave amplitude of the surface waves depend on the properties of liquids and the the falling heights, given in section 2.2.1. In addition, the process of prewetting and the substrate speed also influences the surface waves, as observed in section 2.2.2. The surface waves and their stability are discussed in section 3.
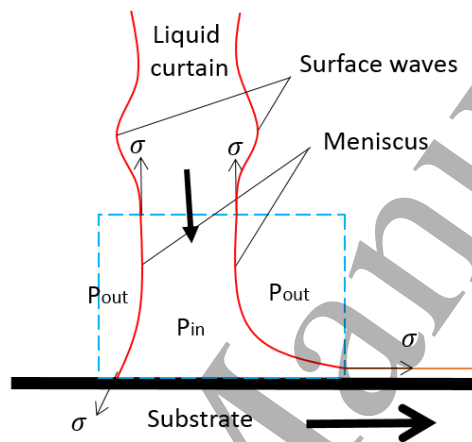
Figure 3. Pressure difference near the meniscus. P_{in} and P_{out}, denote the pressure inside and outside of the meniscus, respectively. σ denotes the surface tension.

Table 1. Captions of parameters in the experiments.

V	Substrate speed
q	Unit discharge
h	Falling height
W:E:G	Water:ethanol:glycerine
Re	Reynolds number
We_{sub}	Weber number above the substrate
Ca_{sub}	Capillary number above the substrate

2.2.1. Roller experiment

Table 2 lists the liquid properties and the experimental conditions in this experiment, which aids in classifying the variation in wave patterns of the surface waves. The liquid is prepared by mixing water, ethanol, and glycerine in four appropriate ratios in order to vary the liquid viscosity and surface tension over a broad range. In these experiments, the positions of experimental setup and lamp are fixed. So the wave crests, wave troughs and wave slopes can be observed through the reflection of light. The wave amplitude cannot be measured directly because the falling height is only several millimeters and the existence of the slot and the substrate also hinders this measurement, so the sensor head to measure the film thickness could not be inserted just above the curtain surface.

Table 2. Experimental conditions with different liquids.

Die width w (cm)		6.0		
Slot width H_I (mm)		0.3		
Unit discharge q (cm^2 s^{-1})		0.227		
Water(W):ethanol(E):glycerine(G) (wt %)	95:5:0	76:4:20	70:20:10	40:40:20
Viscosity μ (cP)	1.11	2.01	2.76	3.97
Surface tension coefficient γ (N m^{-1})	56.7	52.0	34.8	26.3
Density ρ (g cm^{-3})	0.989	1.044	0.830	0.968
Substrate speed V (cm s^{-1})		6.6		
Falling height h (mm)		8.0		
Substrate		Roller		

(a)

(b)

(c)

(d)
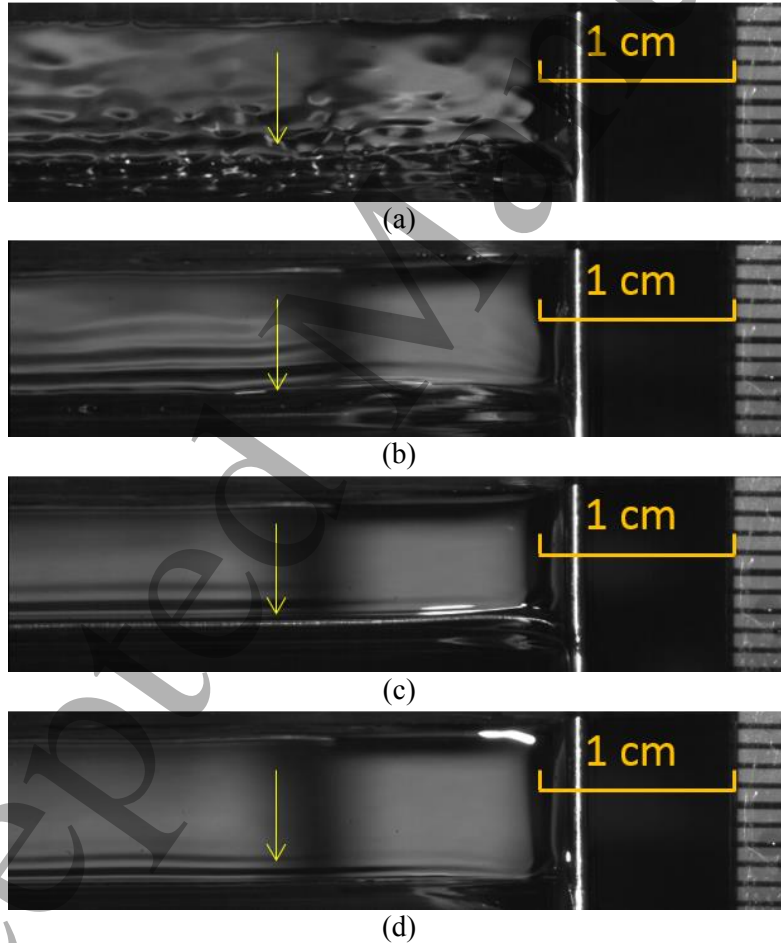
Figure 4. Wave patterns of the surface waves in vertical direction observed in the experiment on a falling liquid curtain onto a roller ($V = 6.6$ cm s^{-1}, $q = 0.227$ cm^2 s^{-1}). (a) W:E:G = 95:5:0, $We_{sub} = 0.16$ 0.16, $Re = 20.2$, $Ca_{sub} = 0.0079$. (b) W:E:G = 76:4:20, $We_{sub} = 0.18$, $Re = 11.8$, $Ca_{sub} = 0.015$. (c) W:E:G = 70:20:10, $We_{sub} = 0.22$, $Re = 6.8$, $Ca_{sub} = 0.032$. (d) W:E:G = 40:40:20, $We_{sub} = 0.34$, $Re = 5.5$, $Ca_{sub} = 0.062$.

5
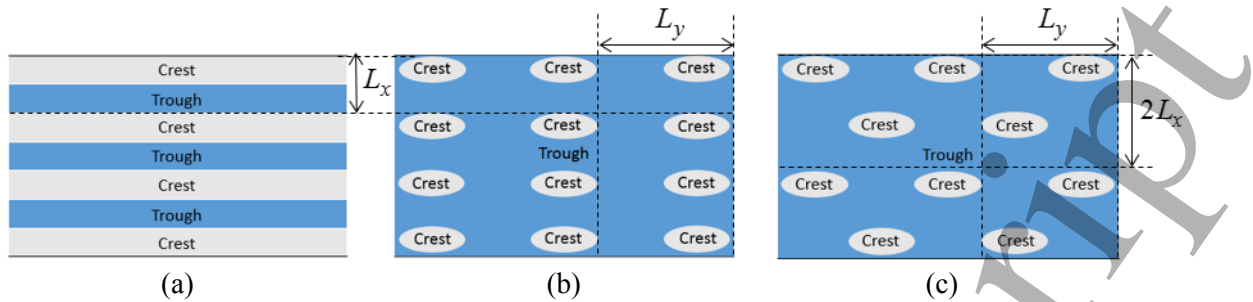
Figure 5. Wave patterns. Here, the x and y coordinates are defined by vertical and horizontal directions, respectively. (a) Straight wave crests with wavelength L_x. (b) Peak-valley wave crests with wavelength L_x and L_y. (c) Staggered wave crests with wavelengths, $2L_x$ and L_y.

Figure 4 shows the curtain surface for the roller experiment with different liquids. Wave patterns observed in the present study are summarized as follows:

(1) Wave number, k: In figure 4, for the several long and narrow zones in the horizontal direction, the bright and dark zones represent the crests and troughs of the surface waves in the vertical direction. The wave-length gradually becomes shorter, in the order as shown from figures (a) to (d), which implies that the wave number k increases with the increase in We_{sub}.

(2) Wave amplitude, A: A cannot be measured directly, but the variation of the wave amplitude can be seen through the photo-images, because the wave steepness can be observed through the differences in brightness between the bright and dark zones due to the reflection of light as shown in figure 4. The wave slopes increase from upstream to downstream for every case, (a), (b), (c), and (d).

(3) Distribution of wave crests: Figure 5 lists three types of wave patterns, namely, straight wave crests, peak-valley wave crests, and staggered wave crests, respectively. The straight and staggered wave crests are observed in our experiment while the peak-valley wave crests are not. For the cases of (b), (c), and (d), they belong to straight wave crests. However, case (a) belongs to staggered wave crests. The modes of peak-valley and staggered waves are investigated in order to explain the instability of the surface waves, and details regarding the same are discussed in section 5.
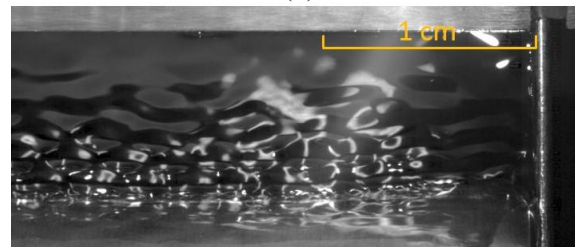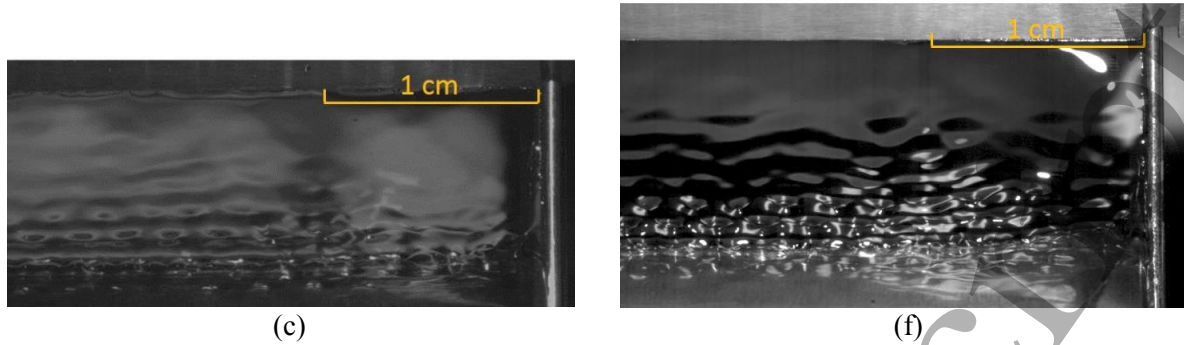

6

(c)   (f)
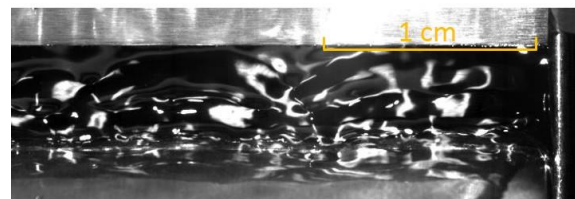
Figure 6. Wave patterns with different unit discharge q and falling height h. (a) $q = 0.227$ cm^2 s^{-1}, $Re = 20.2$, $h = 3$ mm, $We_{sub} = 0.1$, and $Ca_{sub} = 0.0049$. (b) $q = 0.227$ cm^2 s^{-1}, $Re = 20.2$, $h = 5$ mm, $We_{sub} = 0.13$, and $Ca_{sub} = 0.0063$. (c) $q = 0.227$ cm^2 s^{-1}, $Re = 20.2$, $h = 8$ mm, $We_{sub} = 0.16$, and $Ca_{sub} = 0.0079$. (d) $q = 0.955$ cm^2 s^{-1}, $Re = 85.1$, $h = 5$ mm, $We_{sub} = 0.74$, and $Ca_{sub} = 0.0078$. (e) $q = 0.955$ cm^2 s^{-1}, $Re = 85.1$, $h = 8$ mm, $We_{sub} = 0.85$, and $Ca_{sub} = 0.0099$. (f) $q = 0.955$ cm^2 s^{-1}, $Re = 85.1$, $h = 10$ mm, $We_{sub} = 0.91$, and $Ca_{sub} = 0.0107$.

A larger unit discharge and a greater falling height imply that the curtain flow impinges the surface of the substrate at a greater speed. The experimental conditions for this case are listed in table 3. Figure 6 shows the appearance of the liquid curtain with different unit discharge q and falling height h. When the discharge is fixed at a small value ($q = 0.227$ cm^2 s^{-1}) and the falling height is small ($h \leq 3$ mm), the liquid curtain appears smooth without surface waves as shown in figure 6 (a). With the increase in the falling height ($h = 5$ mm), the liquid curtain is less smoother, and the stable surface waves appear on it as shown in figure 6 (b). If the falling height reaches a certain value ($h \geq 8$ mm), the surface waves on the liquid curtain becomes unstable, leading to the staggered wave pattern. It is also observed that the wave number k increases with the increase in the falling height. When the discharge is fixed at a larger value ($q = 0.955$ cm^2 s^{-1}), similar phenomena with different falling heights of the liquid curtain are observed as shown in figure 6 (d), 6 (e) and 6 (f). When the falling height is small ($h \leq 5$ mm) as shown in figure (d), the liquid curtain, in similar state with that in figure 6(b), is not so smooth. If the falling height reaches a certain value ($h \geq 8$ mm) as shown in figure 6 (e) and (f), the surface waves on the liquid curtain becomes unstable and the staggered wave pattern appears, similar with the patterns shown in figure 6(c).

Table 3. Experimental conditions with different falling heights.

Die width w (cm)	6.0
Slot width H_I (mm)	0.3
Unit discharge q (cm^2 s^{-1})	0.227 and 0.955
Water(W):ethanol(E):glycerine(G) (wt %)	95:5:0
Viscosity μ (cP)	1.11
Surface tension coefficient γ (N m^{-1})	56.7
Density ρ (g cm^{-3})	0.989
Substrate speed V (cm s^{-1})	6.6
Falling height h (mm)	3.0, 5.0, 8.0 and 10.0
Substrate	Roller

7

2.2.2. Conveyer belt substrate

In this experiment, we used the mist generator to generate mist. The working process is shown in figure 7. When the mist gets in touch with the surface of the roller, a very thin liquid coating layer forms on the surface of the roller, which we refer to as the pre-wet coating [11]. The discharge of the mist to the substrate is less than 1% of that of the coated liquid. Hence, we can ignore the influence of the pre-wet coating layer on the thickness of the final coating layer. We aim to understand the influence of the pre-wet coating on the surface wave patterns. The experimental conditions for this case are listed in table 4.
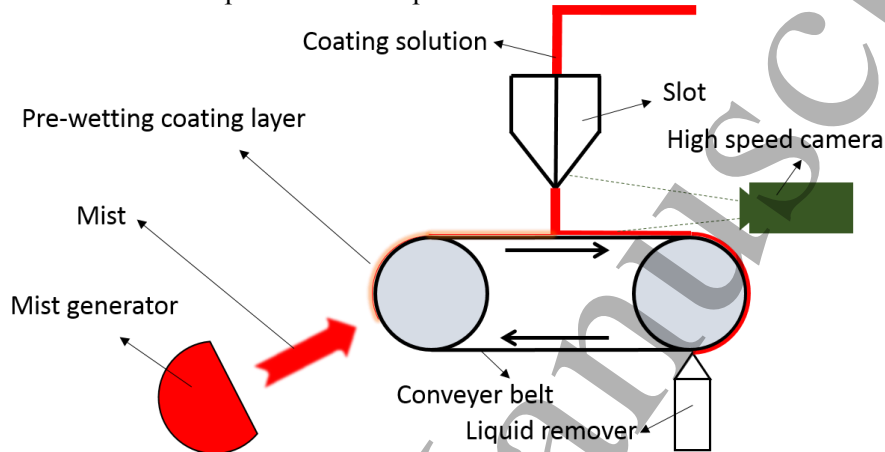
Figure 7. Process of prewetting. The mist generator is Panasonic EH-SA32-P.

Table 4. Experimental conditions for non –pre-wet and pre-wet processes.

Die width w (cm)	6.0
Slot width H_I (mm)	0.3
Unit discharge q (cm^2 s^{-1})	0.268, 0.751 and 1.14
Water(W):ethanol(E):glycerine(G) (wt %)	95:5:0
Viscosity μ (cP)	1.11
Surface tension coefficient γ (N m^{-1})	56.7
Density ρ (g cm^{-3})	0.989
Substrate speed V (cm s^{-1})	45.0
Falling height h (mm)	5.0
Substrate	Conveyer belt

Figures 8 (a), (b), and (c) show the liquid patterns with dry -substrate and pre-wet -substrate. Through comparison, we observe that the steepness of the liquid curtain reduces after pre-wetting. Here, the steepness of the liquid curtain is defined by the ratio of the amplitude to the wavelength of the varicose waves on the liquid curtain. The variation of wave amplitude and wave number of the surface waves are reduced for the pre-wet –substrate as compared to the dry -substrate. The front side of the liquid curtain of figure 8 (b) is shown in figure 8 (d-1). There is a shift of contact line of wetting for the two different substrates. Figure 8 (d-2) contain the images of the side face of the liquid curtains. Compared to a dry -substrate, the angle between the middle liquid surface and the edge guide is lesser for the pre-wet -substrate.

Dry -substrate   Pre-wet -substrate

(a)

(b)

(c)

(d-1)

(d-2)
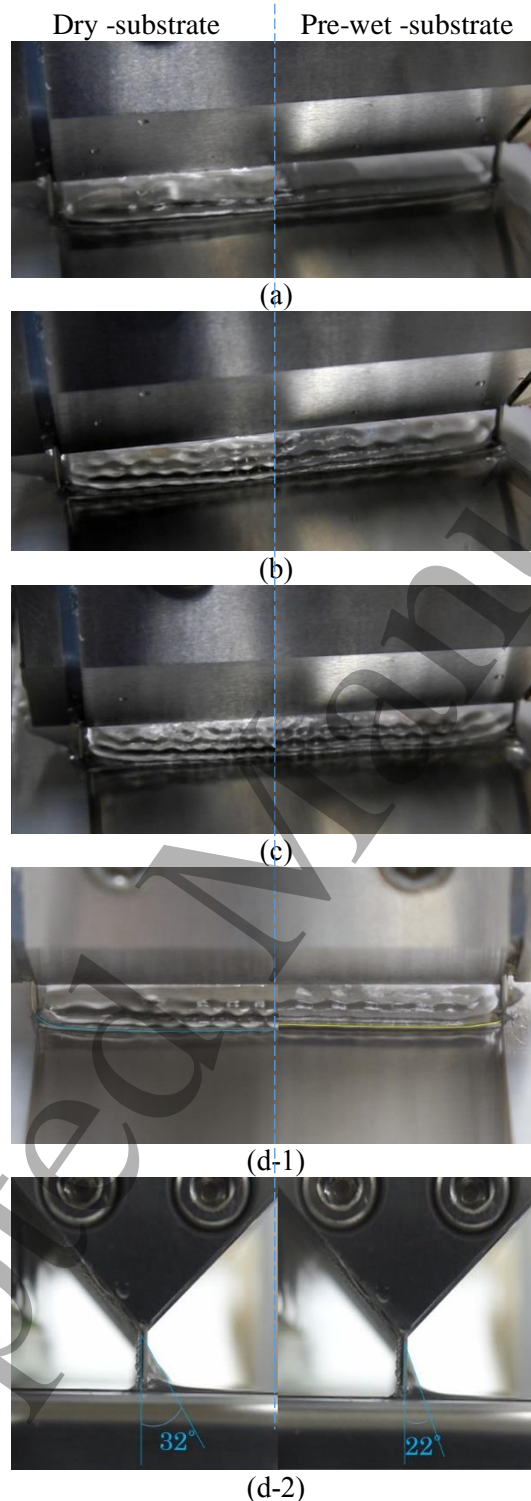
Figure 8. Liquid curtains with dry -substrate and pre-wet -substrate. The left and right sides of the image show the cases for dry and pre-wet substrates, respectively. (a) $q = 0.268$ cm^2 s^{-1}, $We_{sub} = 0.15$, and $Re = 23.9$. (b) $q = 0.751$ cm^2 s^{-1}, $We_{sub} = 0.53$, and $Re = 66.9$. (c) $q = 1.14$ cm^2 s^{-1}, $We_{sub} = 0.98$, and $Re = 101.6$. (d) $q = 0.751$ cm^2/s, $We_{sub} = 0.53$, and $Re = 66.9$. (d-1) The front sides of the liquid curtains. (d-2) The side face of the liquid curtains.

(a) Dry -substrate   (b) Pre-wet -substrate
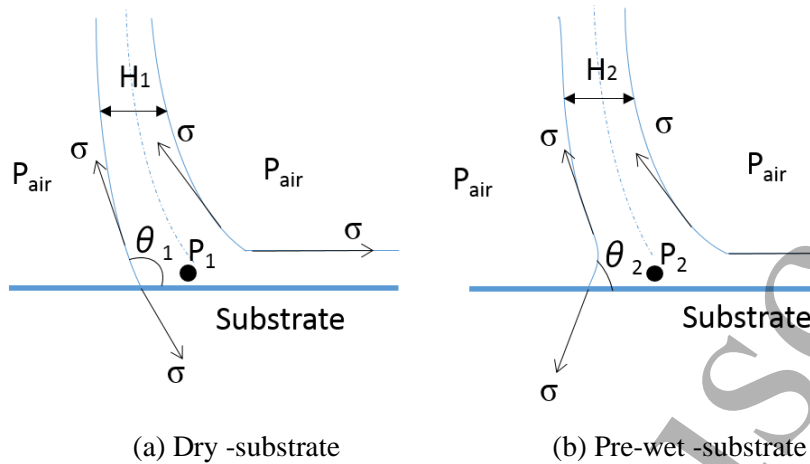
Figure 9. Schematic view of the difference of pressure distribution. (Here, P denotes the pressure inside the meniscus, θ the contact angle and the subscripts '1' and '2' the value for dry -substrate and pre-wet –substrate, respectively.)

The dynamic wetting line should be three-phase with a dry-substrate, which is a gas-liquid-solid system. After pre-wetting, a rather thin liquid coating forms on the surface of moving substrate. So, the dynamic wetting line should be two-phase, which is a gas-liquid system. Compared with three-phase system, two-phase system is wetted more easily, leading to the shift of contact line and change of the angle between the middle liquid surface and the edge guide. The reason for this difference may due to the variation of the pressure distribution as shown in figure 9. The pressure of the liquid curtain near the surface of the substrate is reduced after pre-wetting as the contact angle θ becomes smaller which changes the direction of the surface tension force.

Table 5. Experimental conditions with different substrate speeds.

Die width w (cm)	6.0
Slot width H_I (mm)	0.3
Unit discharge q (cm^2 s^{-1})	0.227
Water(W):ethanol(E):glycerine(G) (wt %)	95:5:0
Viscosity μ (cP)	1.11
Surface tension coefficient γ (N m^{-1})	56.7
Density ρ (g cm^{-3})	0.989
Substrate speed V (cm s^{-1})	9.0, 15.0 and 21.0
Falling height h (mm)	5.0
Substrate	Conveyer belt

10

(a)

(b)

(c)

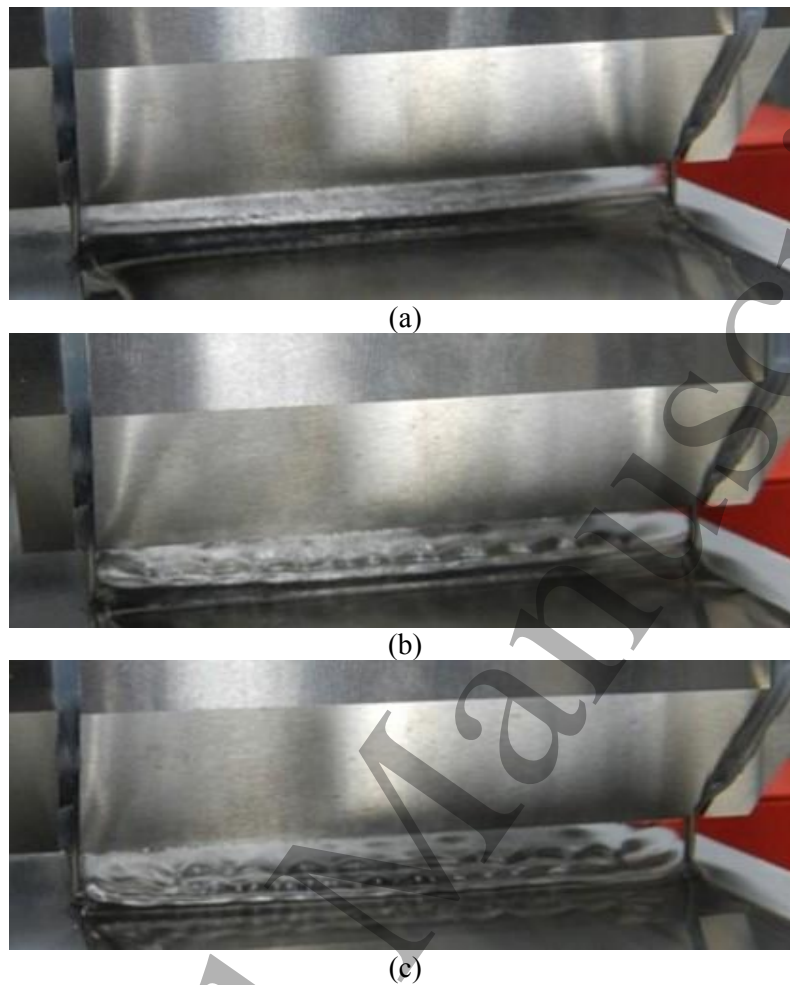**Figure 10.** Different substrate velocities V . Here, $q = 0.497$ cm² s⁻¹, $We_{sub} = 0.31$, and $Re = 44.3$. (a) $V = 0.9$ cm s⁻¹. (b) $V = 1.5$ cm s⁻¹. (c) $V = 2.1$ cm s⁻¹.

The liquid curtain with different substrate speed is shown in figure 10. The experimental condition for this experiment is listed in table 5. The substrate speed increases while the falling height is fixed. When the substrate speed is small ($V = 0.9$ cm s⁻¹), the liquid curtain is smooth and stable as shown in figure 10 (a). As the substrate speed increases, the smoothness is not maintained as the surface waves start to appear on the liquid curtain as shown in figure 10 (b). If the substrate speed continues to increase, the wave number k of the surface waves will also increase as shown in figure 10 (c).

3. Analysis

3.1. Surface waves in the vertical direction

In our experiments, surface waves are observed on the liquid curtain because of existence of the substrate, which lead to a large pressure difference between the inner and outer region of the meniscus on the substrate, and propagate upstream. They are categorised as varicose waves that propagate upstream on the curtain and become stationary because of the downstream flow. In this section, Kistler's equation is used as our governing equation. Here, we obtain the approximate solutions to these equations and try to

11

explain the wave patterns observed in our experiment with respect to them. Finally, we show the results of the numerical simulation using these equations and compare them with the experimental results.

3.1.1. Two dimensional equations governing the curtain profile

The thickness of the liquid curtain observed in our experiment is rather small compared with the wavelength. The governing equation for a stationary liquid curtain in vertical fall on the hypotheses that the ratio of thickness of the liquid curtain and wavelength is much smaller than 1 is given by Kistler [19, 20]. In our experiment, the angle between the mid surface and the horizontal direction is observed to be 90 ° because the roller velocity V is small, which implies that the mid surface of the liquid curtain is not viewed as a curve, but as a straight line in the vertical direction. The governing equation is given as follows:

$$-\frac{Re}{\tilde{H}^3}\frac{d\tilde{H}}{d\tilde{x}} - \frac{4}{\tilde{H}^3}\left(\left(\frac{d\tilde{H}}{d\tilde{x}}\right)^2 - \tilde{H}\frac{\mathrm{d}^2\tilde{H}}{\mathrm{d}\tilde{x}^2}\right) - \frac{1}{2Ca}\frac{\mathrm{d}^3\tilde{H}}{\mathrm{d}\tilde{x}^3} - Fr^{-2}Re = 0 \tag{1}$$

The first, second, third, and last terms represent the inertial force, the viscous term, the surface tension, and the gravity term, respectively. Here, H denotes the thickness of the liquid curtain and x denotes the distance from the slot die along the curtain mid surface to the end of the liquid curtain in the downstream direction. In addition, ' ~ ' denotes the dimensionless parameter, non-dimensionalised by the typical length scale, L. Re, Ca, and Fr denote the Reynolds number, the Capillary number and the Froude number, respectively; they are respectively defined as:

$$Re = \frac{\rho U L}{\mu}, \ Ca = \frac{\mu U}{\gamma}, \ Fr = \frac{U}{\sqrt{Lg}} \tag{2}$$

Here, ρ, U, γ, and g denotes the liquid density, the liquid velocity, μ the viscosity, the surface tension, and the acceleration due to gravity, respectively.

3.1.2. Local linear analysis
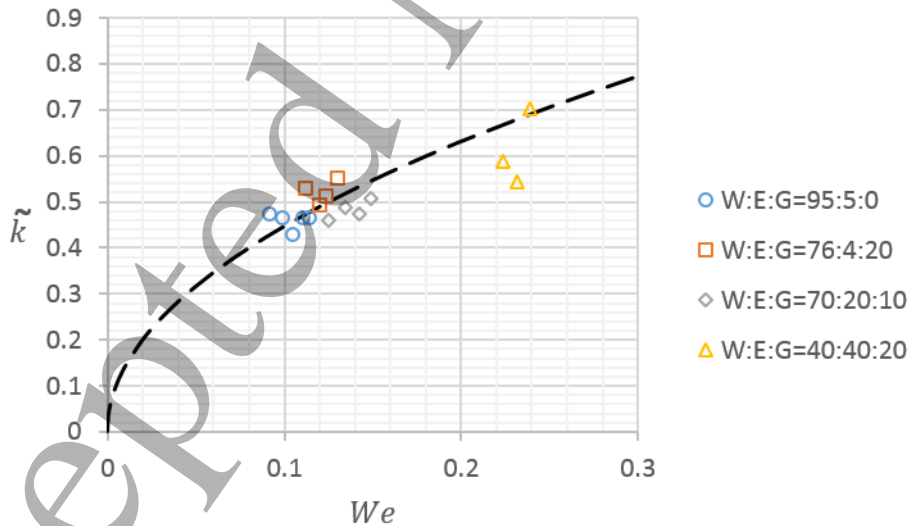
Figure 11. Non-dimensional wave number $\tilde{k}$ plotted as a function of We for various liquids in our experiment of a falling liquid curtain onto a roller. Symbols denote different liquids for each experimental data point, as listed in the legend. The dashed line denotes equation (8). Here, $K = 0.8$ is used to represent a smooth approximation of experimental data.

By the perturbation method, the approximate solution to equation (1) can be given by

$$\tilde{H}(\zeta,\tilde{x}) = 1 + \zeta H_f(\tilde{x}) \tag{3}$$

in terms of the parameter ζ which represents the order of the amplitude of the waves on the liquid curtain. Here, we choose the local curtain thickness $H_s(x)$ and velocity $U_s(x)$ as the typical length scale L and velocity U, respectively. By taking into account the order of ζ, the simplified equation (3) is obtained:

$$\frac{d^2 H_f}{d\tilde{x}^2} - 8Ca\frac{dH_f}{d\tilde{x}} + 2WeH_f = 0. \tag{4}$$

This is a second-order linear ordinary differential equation. Its general solution is given by:

$$H_f(\tilde{x}) = e^{4Ca(\tilde{x}-\tilde{h})}\sin\left(\sqrt{2We}\sqrt{1-\frac{8We}{Re^2}}\tilde{x}\right). \tag{5}$$

Here, the wave amplitude at the bottom of the liquid curtain is considered to be unit. In our experiment, as $\dfrac{We}{Re^2} \ll 1$, equation (6) can be rewritten by:

$$H_f(\tilde{x}) = e^{4Ca(\tilde{x}-\tilde{h})}\sin\left(\sqrt{2We}\tilde{x}\right). \tag{6}$$

According to equation (6), we can conclude that the disturbance decays upstream and the Capillary number Ca determines the decay rate. Moreover, the non-dimensional wave number $\tilde{k}$ depends on the Weber number We.

$$\tilde{k} = \sqrt{2We} \tag{7}$$

It should be noted that both Ca and We decrease upstream as the liquid velocity $U(x)$ decreases upstream.

In figure 11, the comparison of the wave numbers and Weber numbers of experimental and theoretical data are shown. With Weber number increases, the wave number also increases. The non-dimensional wave number $\tilde{k}$ for the experimental data is given by:

$$\tilde{k} = \frac{2\pi H_s}{\lambda}, \tag{8}$$

where the wave length λ is measured by Photron FASTCAM Viewer 3, and the curtain thickness H_s is given by

$$H_s(x) = \frac{q}{U_s(x)}. \tag{9}$$

Here, $U_s(x)$ is substituted as

$$U_s(x) = KU_B(x), \tag{10}$$

where U_B is derived from Bernoulli's theorem as follows:

$$U_B(x) = \sqrt{U_0^2 + 2gx}, \quad U_0 = \frac{q}{H_I}. \tag{11}$$

In addition, K denotes the ratio of liquid velocities obtained by calculating the rate of change of position with respect to time and estimated by Bernoulli's theorem. In our experiment, tracer-particles are put in the liquid and their traces are recorded by high speed camera as shown in figure 12 (a) and (b). The velocities are obtained by calculating the rate of change of position with respect to time. The figure 12 (c) shows the data of the velocities of the particle. $K = 0.8$ can represent the velocities well generally. The value of K is less than 1 due to the viscosity effect and the wave generation. So, the measured velocity is always smaller than $U_B(x)$. The particle velocity fluctuates around the curve of $K = 0.8$

because of the existence of the surface waves. By using these data, the thickness variation upstream are estimated (0.07 mm ~ 0.3 mm) from the continuity of unit discharge. The figure 13 explain the method employed to measure the averaged wavelengths, which represent the experimental data in figure 11.

(a)

(b)

(c)
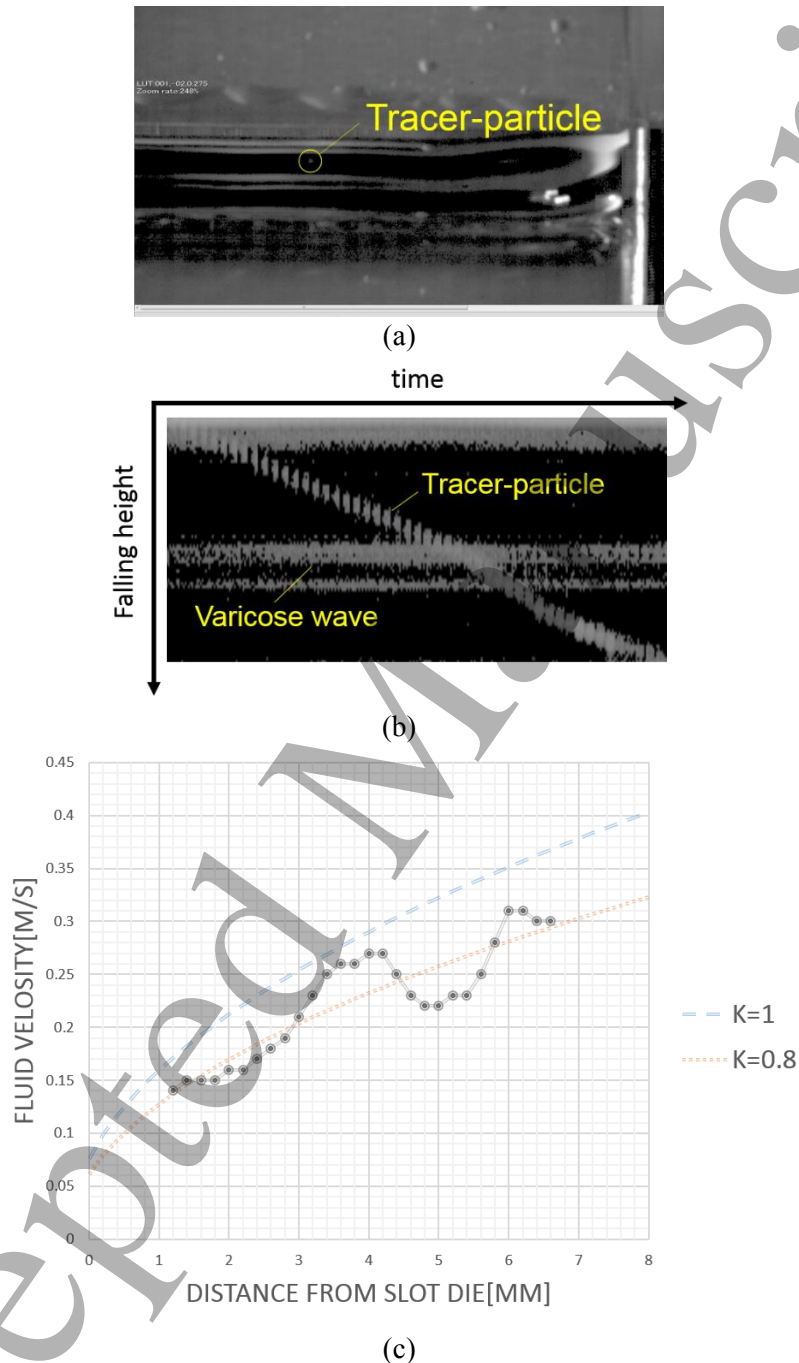
Figure 12. Liquid velocities obtained by calculating the rate of change of position with respect to time. (W:E:G = 70:20:10, $V = 0$ cm s^{-1}, $q = 0.227$ cm^2 s^{-1}) (a) Tracer-particles in the liquid curtain. The mean diameter of these tracer-particles is 15 μm. (b)Trace of particle in the liquid curtain. The pictures of the tracer-particle in different times are joined together from left to right. (c) The velocity of the tracer-particle.
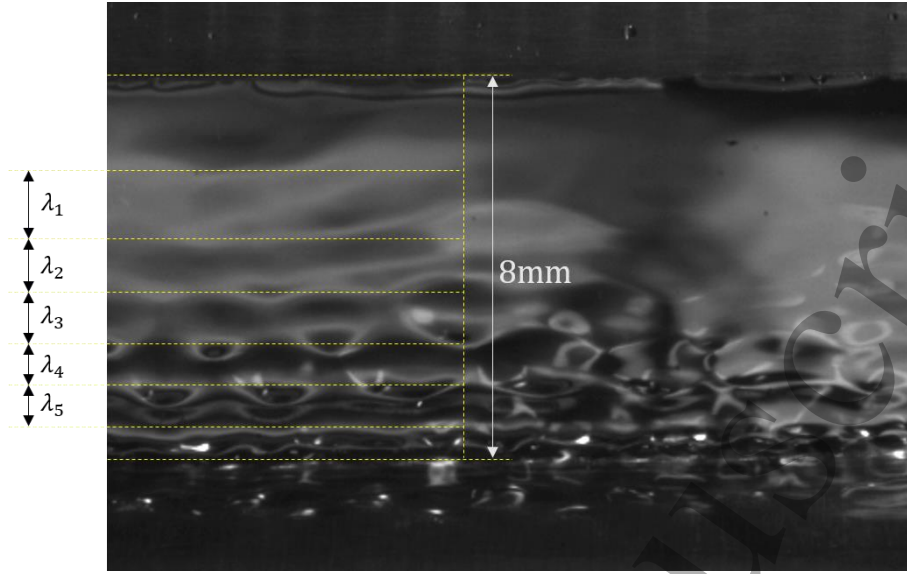
14

Figure 13. The method to obtain the wavelength. λ_1, λ_2, λ_3, λ_4 and λ_5 are measured as the mean wavelengths as the fluctuation of these surface waves is small compared with them (W:E:G = 95:5:0, $V = 6.6 \text{ cm s}^{-1}$, $q = 0.227 \text{ cm}^2 \text{ s}^{-1}$).

According to previous study [21], there are two types of waves propagating in a liquid curtain, i.e. sinuous and varicose waves, which have the following celerity:

$$C_{sin} = \sqrt{\frac{2\gamma}{\rho H_s(x)}} \tag{12}$$

$$C_{var} = \sqrt{\frac{\gamma H_s(x)}{2\rho}}k, \ k \equiv \frac{2\pi}{\lambda}, \tag{13}$$

respectively. Here, ρ, γ, H, and k denote the liquid density, the surface tension coefficient, the curtain thickness and the wave number, respectively. The waves observed in our experiment are stationary; therefore, we could obtain the wave velocity, which is equal to the liquid velocity everywhere in the vertical direction, i.e.

$$U_s(x) = C_{var} \tag{14}$$

which leads to equation (8). Hence, the surface waves in our experiment are varicose waves.

3.1.3. Numerical analysis
In our experiment, the flow of liquid curtain is divided into two zones, namely, falling and impingement zones (or symmetric and asymmetric zones) as shown in figure 14. The falling zone can be viewed as a symmetrical mode, while the impingement zone is asymmetrical mode. Equation (1) can be solved under the boundary conditions of $\tilde{x} = 0$ and $\tilde{x} = \tilde{h}$ as follows:

$$\tilde{H}(0) = 1, \ \frac{d\tilde{H}(\tilde{h})}{d\tilde{x}} = a, \ \frac{d^2\tilde{H}(\tilde{h})}{d\tilde{x}^2} = b \tag{15}$$

where $\tilde{h}$ denotes the non-dimensional distance from the slot die to the bottom of the falling zone normalized by the die widths H_I; a and b represent the meniscus angle and the pressure inside the meniscus, respectively. Though a and b can be determined from the flow in the impingement zone, we assume these values and discuss a general behaviour of the curtain as a whole.
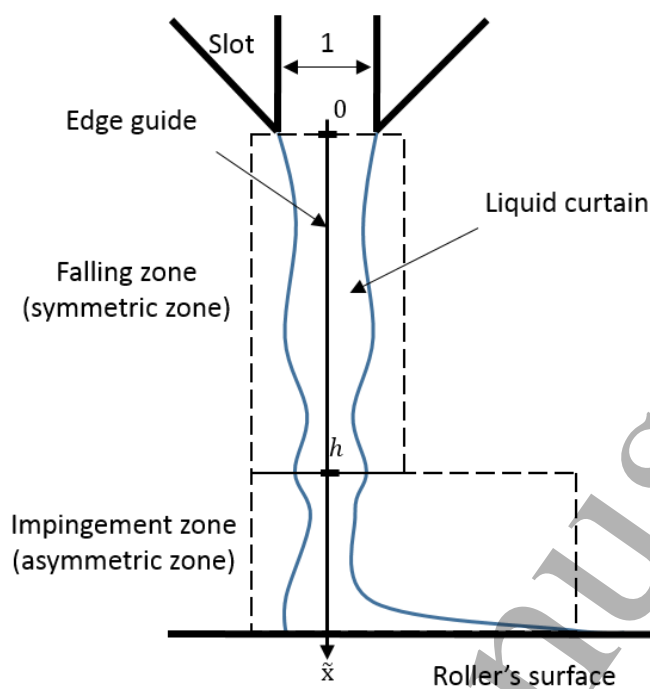
15

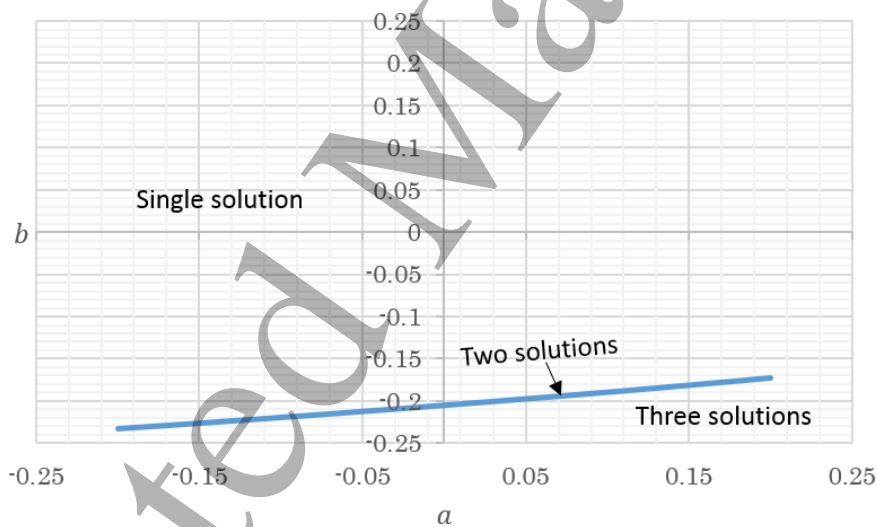**Figure 14.** Flow zones in our experiment.

Figure 15. The number of solutions depends on the values of a and b. The coloured line represents the boundary between the single and three solutions. The regions on the upper and lower sides of the line represent the cases of single and three solutions, respectively.
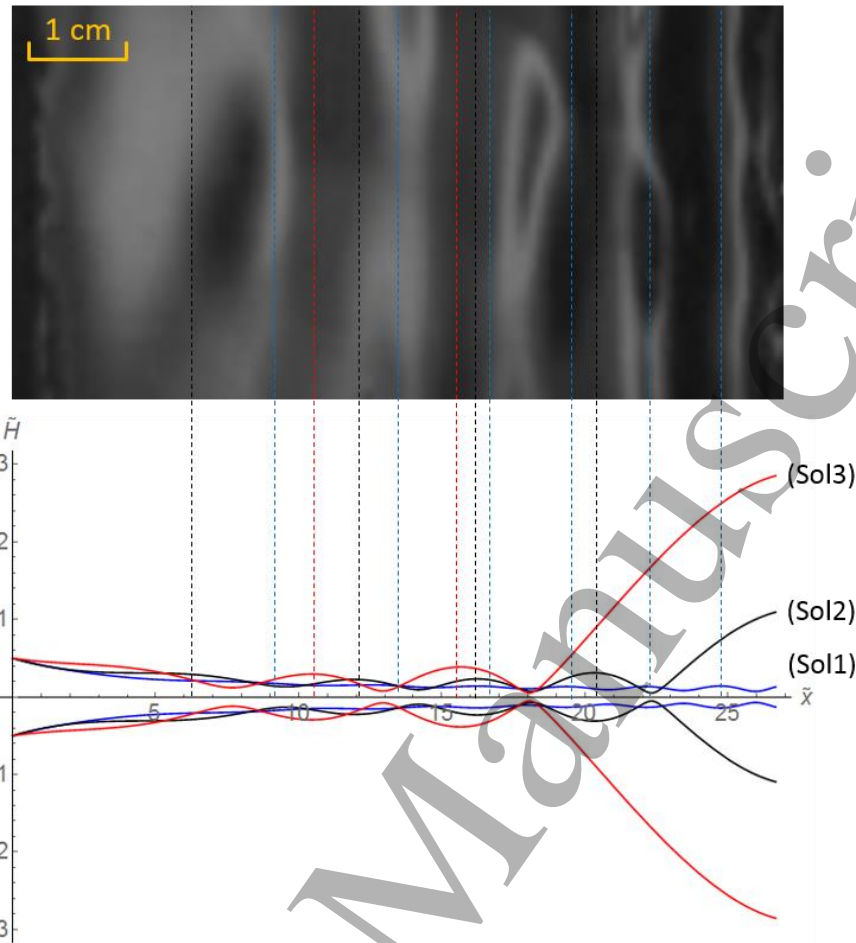
Figure 16. Multiple solutions of curtain profiles with the same values of, a and b, i.e. $a = 0.2$, $b = -0.2$, and W:E:G = 95:5:0. $\tilde{x}$ is scaled by the slot width H_I, 0.3 mm.

Table 6. The thicknesses of liquid curtain at the bottom of it under different boundary conditions.

a	b	$\tilde{H}(0)$	$\tilde{H}(\tilde{h})$
	-0.18		0.24
0.1	-0.19		0.24 and 3.91
	-0.25	1	0.24, 2.60 and 5.02
	-0.18		0.24
-0.1	-0.22		0.24 and 3.39
	-0.25		0.24, 1.92 and 7.09

In the present study, we fix the value of a and use a shooting method to find the value of b which fits the boundary condition at the die exit, i.e. $\tilde{H}(0) = 1$. A similar method has been employed in another paper [13]. Moreover, we find that even under the same boundary conditions, there may be more than one solution to equation (3), which implies that besides the given boundary conditions, the curtain profile also depends on other conditions. Table 6 lists a plot of the thicknesses of liquid curtain at the bottom of it under different boundary conditions. Figure 15 shows the number of solutions in the a-b plane. Furthermore, an example of the curtain profiles corresponding to multiple solutions is shown in

17

figure 16. The curtain profile (Sol1) fits the experimental data well while (Sol2) and (Sol3) do not, especially near the bottom of the liquid curtain where the mean thickness is less than that at the top in the experiments. The existence of these two patterns imply that different curtain profiles are possible under some experimental conditions in the impingement zone, such as whether the roller is stationary or in movement.

3.1.4. Numerical solutions

Assuming the values of a and b, equation (3) is solved numerically. Figure 17 shows the numerical solutions corresponding to our experimental conditions. Here, we set a as 0.1 and use the shooting method to find the value of b which fits the experiment data well. Comparing with the wave patterns shown in figure 3, it is obtained that the simulation results shown in figure 17 can explain them well. In addition, we have checked that the magnitude of a and b are not sensitive to the varicose wave profile.

(a)   (b)

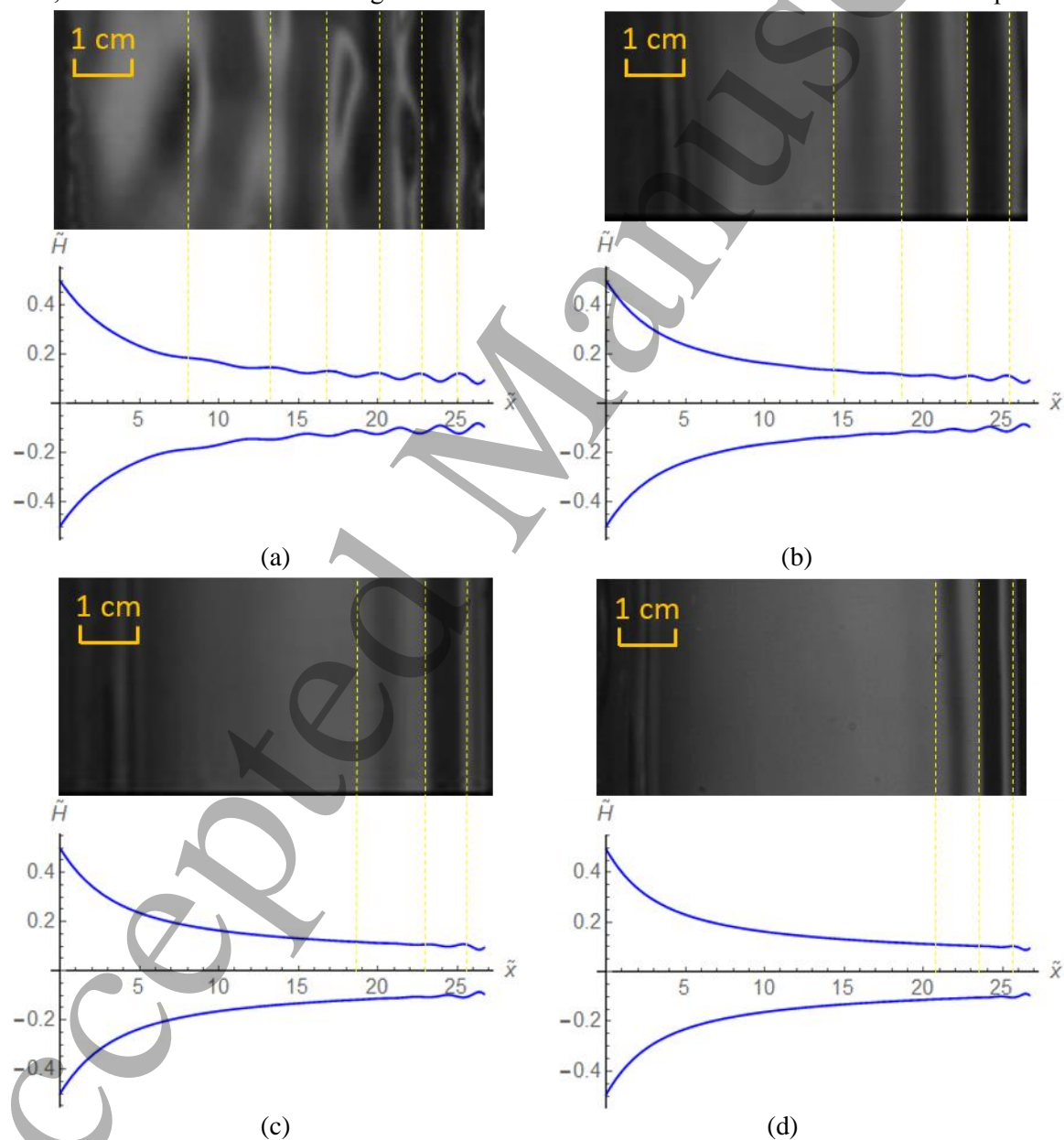(c)   (d)

Figure 17. Numerical solutions of curtain profiles under the boundary conditions compared with experimental images. $\tilde{x}$ is scaled by the slot width H_I, 0.3 mm. (a) for $a = 0.1, b = 0.12$, W:E:G =

18

95:5:0. (b) for $a = 0.1$, $b = 0.17$, W:E:G = 76:4:20. (c) for $a = 0.1$, $b = 0.26$, W:E:G = 70:20:10. (d) for $a = 0.1$, $b = 0.42$, W:E:G = 40:40:20.

3.2. Stability of the varicose waves

3.2.1. Three dimensional equations governing the curtain profile

The equations governing the two-dimensional shape of a soap film have been derived by Chomaz [22]. Considering that the liquid curtain is stationary in our experiments, these governing equations are given as follows

$$
\begin{cases}
\tilde{\boldsymbol{u}} \cdot \nabla \tilde{\boldsymbol{u}} = \dfrac{1}{2We} \nabla \nabla^2 \tilde{H} + Re^{-1} \nabla^2 \tilde{\boldsymbol{u}} + 3 Re^{-1} \nabla \nabla \cdot \tilde{\boldsymbol{u}} + \dfrac{Re^{-1}}{\tilde{H}} \tilde{\boldsymbol{V}} + Fr^{-2} \mathbf{e}_x = 0 \\
\nabla \cdot \left(\tilde{H} \tilde{\boldsymbol{u}} \right) = 0
\end{cases}
\tag{16}
$$

where vector $\tilde{\boldsymbol{V}} = \left(\tilde{V}_x, \tilde{V}_y \right)$ represents additional viscous terms given by

$$
\begin{cases}
\tilde{V}_x = 2 \dfrac{\partial \tilde{H}}{\partial \tilde{x}} \left(2 \dfrac{\partial \tilde{u}}{\partial \tilde{x}} + \dfrac{\partial \tilde{v}}{\partial \tilde{y}} \right) + \dfrac{\partial \tilde{H}}{\partial \tilde{y}} \left(\dfrac{\partial \tilde{u}}{\partial \tilde{y}} + \dfrac{\partial \tilde{v}}{\partial \tilde{x}} \right) \\
\tilde{V}_y = 2 \dfrac{\partial \tilde{H}}{\partial \tilde{y}} \left(\dfrac{\partial \tilde{u}}{\partial \tilde{x}} + 2 \dfrac{\partial \tilde{v}}{\partial \tilde{y}} \right) + \dfrac{\partial \tilde{H}}{\partial \tilde{x}} \left(\dfrac{\partial \tilde{u}}{\partial \tilde{y}} + \dfrac{\partial \tilde{v}}{\partial \tilde{x}} \right)
\end{cases}
\tag{17}
$$

Here, ' $\sim$ ' denotes the dimensionless parameter. The curtain thickness $\tilde{H}$, falling height $\tilde{x}$, and horizontal position $\tilde{y}$ are non-dimensionalised by L, the typical length scale, and the flow velocity $\tilde{\boldsymbol{u}} = (\tilde{u}, \tilde{v})$ is non-dimensionalised by

$$
U_L = \frac{q}{L}
\tag{18}
$$

where q denotes the unit discharge.

If we only consider the variation of the curtain thickness in the vertical direction $\tilde{x}$ in the steady state and ignore the terms of $\tilde{y}$, equation (16) reduces to Kistler's equation (1).
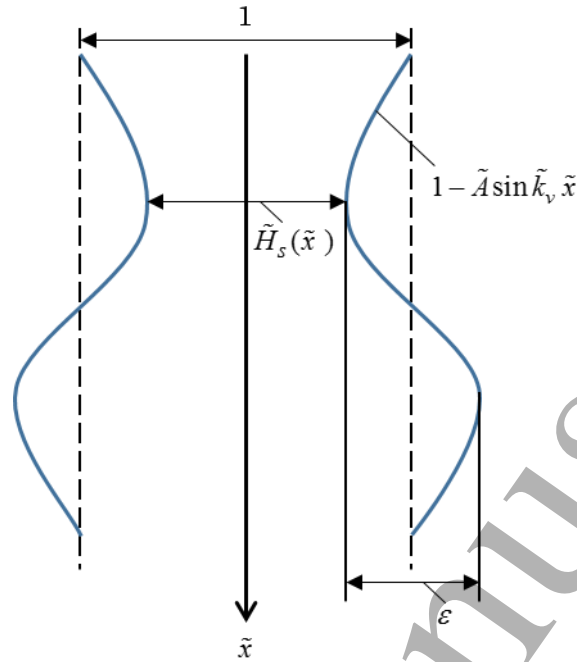
Figure 18. The model of the of local curtain shape.

3.2.2. Disturbance equations

The surface waves on the liquid curtain are varicose waves and the wave crests are uniform as shown in figure 4 (a). However, the type will not always remain the same when the experimental conditions are changed. The staggered type, a peculiar way in which wave crests are distributed as shown in figure 4 (b), is observed in our experiment.

Our experimental observations show that different paths can lead from steady two-dimensional varicose waves to unsteady three-dimensional ones [23]. These paths are distinguished by the nature of three-dimensional disturbances that result in different characteristic wave patterns, as emulated in figure 4. The commonly observed path leads to spanwise alternating 'peak' and 'valleys', i.e. regions of enhanced and reduced disturbance amplitudes, which are associated with a mean longitudinal wave crest of varicose waves.

In order to simply the model of the local shape of the varicose waves, the solutions of curtain thickness in the steady state is substituted in

$$\tilde{H}_s\left(\tilde{x}\right) = 1 - \tilde{A}\sin\tilde{k}_v\tilde{x} \tag{19}$$

which is shown in figure 18. Here, $\tilde{A}$ and $\tilde{k}_v$ represents the amplitude and the streamwise wave number of the varicose waves in the vertical direction, respectively. The variation in the thickness of the liquid curtain remains the same pattern everywhere in the vertical direction, and the falling height is not considered in this model. In addition, time is not considered as it is in the steady state. In order to express the solutions easily in the next step, the coordinate is transformed using

$$\tilde{k}_v\tilde{x} = 2\tilde{x}_L \ . \tag{20}$$

Superposition of small three-dimensional disturbances to the base flow in the form

$$
\begin{cases}
\tilde{H} = \tilde{H}_s\left(\tilde{x}_L\right) + \delta\,\tilde{H}_\varepsilon\left(\tilde{x}_L, \tilde{y}\right) \\
\tilde{u} = \dfrac{1}{\tilde{H}_s\left(\tilde{x}_L\right)} + \delta\,\tilde{u}_\varepsilon\left(\tilde{x}_L, \tilde{y}\right) \\
\tilde{v} = \delta\,\tilde{v}_\varepsilon\left(\tilde{x}_L, \tilde{y}\right)
\end{cases}
\tag{21}
$$

is substituted into equation (16), and linearize these equations with respect to δ, then the disturbance equations with coefficients independent of $\tilde{y}$ is obtained. Here, δ is a perturbation parameter and ε denotes the disturbance. We therefore assume disturbances in the form

$$
\begin{cases}
\tilde{H}_\varepsilon\left(\tilde{x}_L, \tilde{y}\right) = \tilde{h}_f\left(\tilde{x}_L\right)e^{ik\tilde{y}} \\
\tilde{u}_\varepsilon\left(\tilde{x}_L, \tilde{y}\right) = \tilde{u}_f\left(\tilde{x}_L\right)e^{ik\tilde{y}} \\
\tilde{v}_\varepsilon\left(\tilde{x}_L, \tilde{y}\right) = \tilde{v}_f\left(\tilde{x}_L\right)e^{ik\tilde{y}}
\end{cases}
\tag{22}
$$

The resulting disturbance equations have periodic coefficients owing to the periodic base flow due to varicose waves. The equations are essentially of Hill type with damping [24]. Such systems permit various classes of solutions; the two most important classes arise from primary resonance with wavelength L_x and from principal parametric resonance with wavelength $2L_x$.

Principal parametric resonance generates the modes of instability that are associated with staggered pattern, for which we can obtain disturbances using

$$
\begin{cases}
\tilde{h}_f\left(\tilde{x}_L\right) = \displaystyle\sum_{n=1}^{n_f}\left\{H_c[n]\cos\left[(2n-1)\tilde{x}_L\right] + H_s[n]\sin\left[(2n-1)\tilde{x}_L\right]\right\} \\
\tilde{u}_f\left(\tilde{x}_L\right) = \displaystyle\sum_{n=1}^{n_f}\left\{U_c[n]\cos\left[(2n-1)\tilde{x}_L\right] + U_s[n]\sin\left[(2n-1)\tilde{x}_L\right]\right\} \\
\tilde{v}_f\left(\tilde{x}_L\right) = \displaystyle\sum_{n=1}^{n_f}\left\{V_c[n]\cos\left[(2n-1)\tilde{x}_L\right] + V_s[n]\sin\left[(2n-1)\tilde{x}_L\right]\right\}
\end{cases}
\tag{23}
$$

Applying equations (19)-(23) to governing equations (16)-(17), after linearization in δ, results in a $6n_f \times 6n_f$ matrix eigenvalue problem for We, Re, $\tilde{A}$, and $\tilde{k}$ in the form

$$\mathbf{M}_a \mathbf{X}_s = \begin{bmatrix} a_{11} & \cdots & a_{16n_f} \\ \vdots & \ddots & \vdots \\ a_{6n_f 1} & \cdots & a_{6n_f 6n_f} \end{bmatrix} \begin{bmatrix} H_c[1] \\ \vdots \\ H_c[n_f] \\ H_s[1] \\ \vdots \\ H_s[n_f] \\ U_c[1] \\ \vdots \\ U_c[n_f] \\ U_s[1] \\ \vdots \\ U_s[n_f] \\ V_c[1] \\ \vdots \\ V_c[n_f] \\ V_s[1] \\ \vdots \\ V_s[n_f] \end{bmatrix} = \mathbf{0} \tag{24}$$

where a_{ij} ($1 \le \mathrm{i} \le 6n_f$, $1 \le \mathrm{j} \le 6n_f$) are functions of We, Re, $\tilde{A}$, and $\tilde{k}$. The existence of the solutions depends on $|\mathbf{M}_a| = 0$. We examine the existence of $\tilde{k}$ when $|\mathbf{M}_a| = 0$ with suitable We, Re, and $\tilde{A}$ values. Figure 19 (a-1) and (a-2) show the stability of the liquid curtain with varicose waves in the Re -We plane considering the amplitude $\tilde{A}$ of the varicose waves. With a larger amplitude $\tilde{A}$, the liquid curtain is more unstable and tend to become staggered pattern mode more easily. This instability occurs when $We \ge 0.25$ at $\tilde{A} = 0.3$, and $We \ge 0.5$ at $\tilde{A} = 0.05$. In our experiment, $We < 1$ and $5 < Re < 90$, so the instability of staggered pattern mode may appear and has been observed as shown in figure 4 (a). With a fixed Reynolds number ($Re = 20.2$ or $Re = 85.1$), the appearance of the liquid curtain transforms form the no-staggered mode to the staggered mode as the Weber number increases.

Primary resonance generates the modes of instability that are associated with peak-valley splitting, for which we can obtain the disturbances using

$$\begin{cases} \tilde{h}_f(\tilde{x}_L) = \sum_{n=0}^{n_f} \{ H_c[n]\cos[2n\tilde{x}_L] + H_s[n]\sin[2n\tilde{x}_L] \} \\ \tilde{u}_f(\tilde{x}_L) = \sum_{n=0}^{n_f} \{ U_c[n]\cos[2n\tilde{x}_L] + U_s[n]\sin[2n\tilde{x}_L] \} \\ \tilde{v}_f(\tilde{x}_L) = \sum_{n=0}^{n_f} \{ V_c[n]\cos[2n\tilde{x}_L] + V_s[n]\sin[2n\tilde{x}_L] \} \end{cases} \tag{25}$$

22

Applying equations (19)-(22) and (25) to governing equations (16)-(17), after linearization in δ, results in a $6(n_f + 1) \times 6(n_f + 1)$ matrix eigenvalue problem for We, Re, $\tilde{A}$, and $\tilde{k}$ in the form

$$\mathbf{M}_b \mathbf{X}_p = \begin{bmatrix} b_{11} & \cdots & b_{1\left(6n_f+1\right)} \\ \vdots & \ddots & \vdots \\ b_{\left(6n_f+1\right)1} & \cdots & b_{\left(6n_f+1\right)\left(6n_f+1\right)} \end{bmatrix} \begin{bmatrix} H_c[0] \\ \vdots \\ H_c[n_f] \\ H_s[0] \\ \vdots \\ H_s[n_f] \\ U_c[0] \\ \vdots \\ U_c[n_f] \\ U_s[0] \\ \vdots \\ U_s[n_f] \\ V_c[0] \\ \vdots \\ V_c[n_f] \\ V_s[0] \\ \vdots \\ V_s[n_f] \end{bmatrix} = \mathbf{0}$$

(26)

where b_{ij} ($1 \le i \le 6(n_f + 1)$, $1 \le j \le 6\left(n_f + 1\right)$) are functions of We, Re, $\tilde{A}$ and $\tilde{k}$. The existence of the solutions depends on $\left|\mathbf{M}_b\right| = 0$. We examine the existence of $\tilde{k}$ when $\left|\mathbf{M}_b\right| = 0$ with suitable We, Re and $\tilde{A}$ values. Figure 19 (b) shows the stability of the liquid curtain with varicose waves in the Re - We plane considering the amplitude $\tilde{A}$ of the varicose waves. The instability of peak-valley mode, occurring when $We \ge 1.5$ and $Re \ge 142$ at $\tilde{A} = 0.3$, are not observed, as We and Re in our experiment are not in the required range. In our experiment, the amplitude $\tilde{A}$ of the varicose waves could not be measured directly, but the steepness is seen from the light reflection. Figure 20 shows the examples of the numerical simulation for the wave patterns with $\tilde{k}$ and suitable We, Re, and $\tilde{A}$ when $\left|\mathbf{M}_a\right| = 0$ or $\left|\mathbf{M}_b\right| = 0$.

23
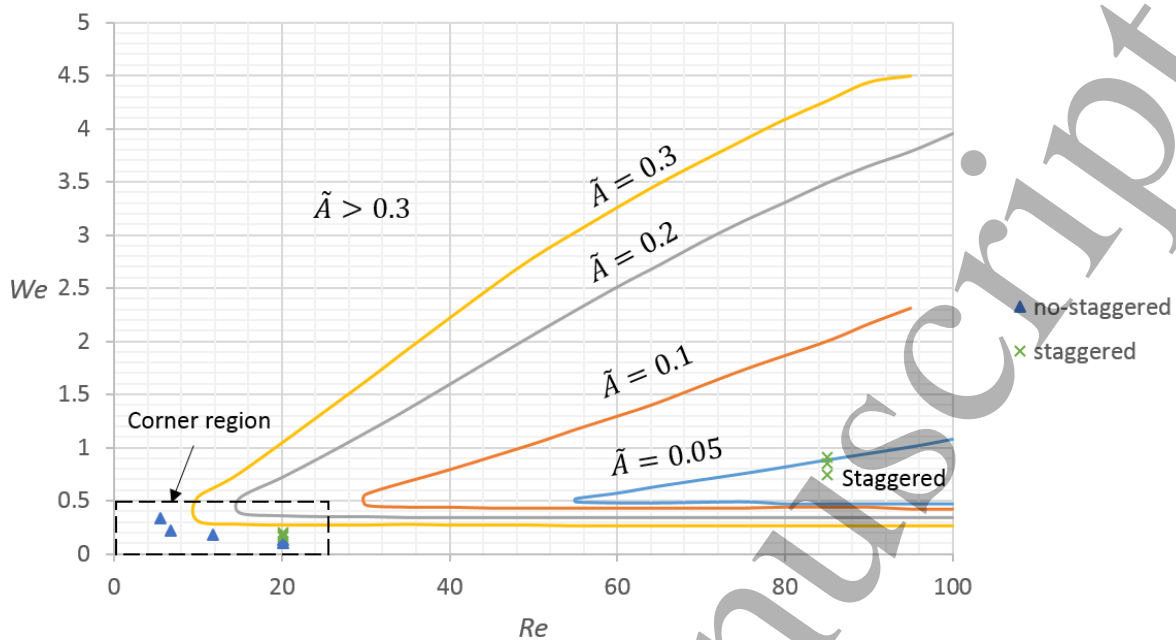
(a-1)
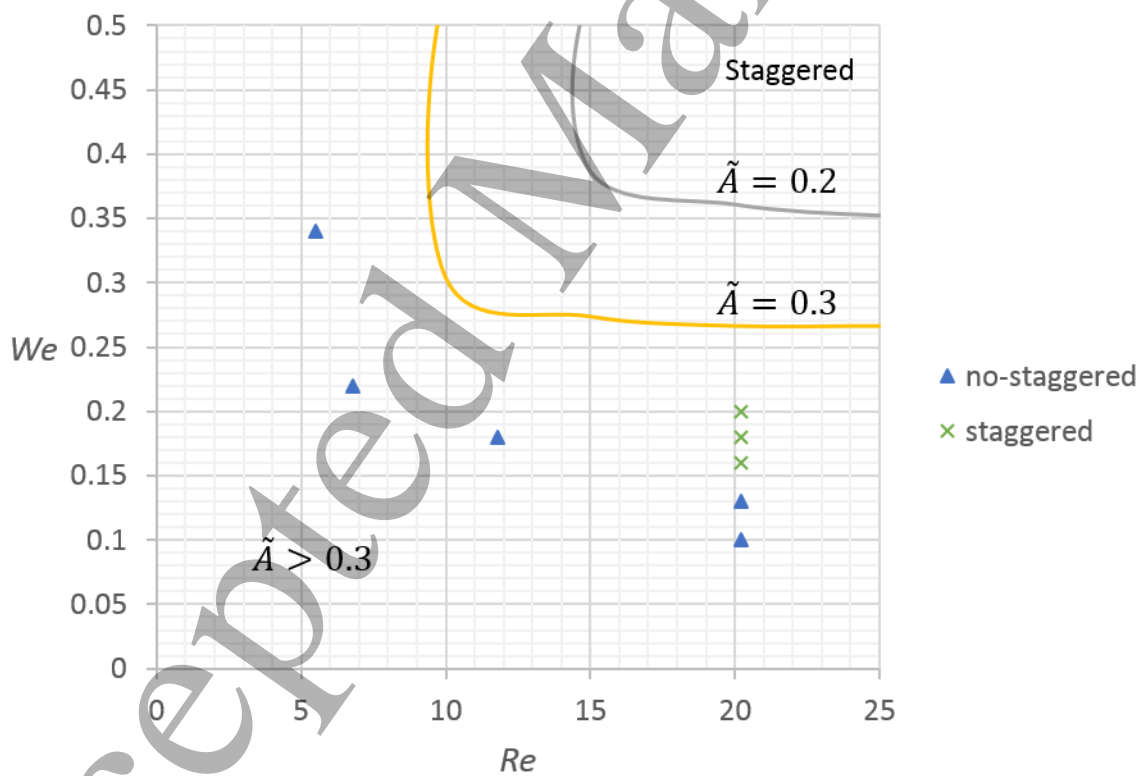
(a-2)
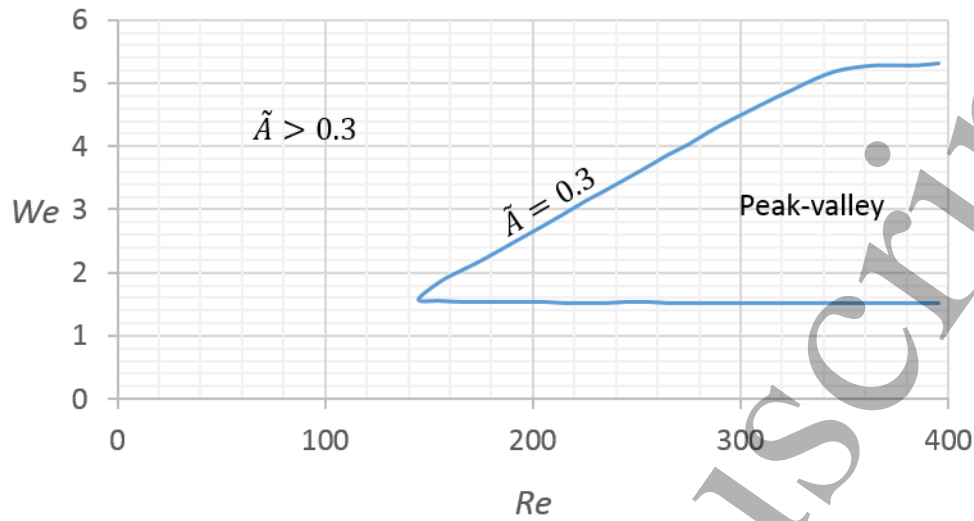
(b)

Figure 19. The instability of the varicose waves on the liquid curtain for two-dimensional disturbance. The triangle and cross represent the no-staggered and staggered mode in the experimental results, respectively. (a-1) Staggered pattern mode. (a-2) Enlarged picture of 'Corner region' in (a-1). (b) Peak-valley mode
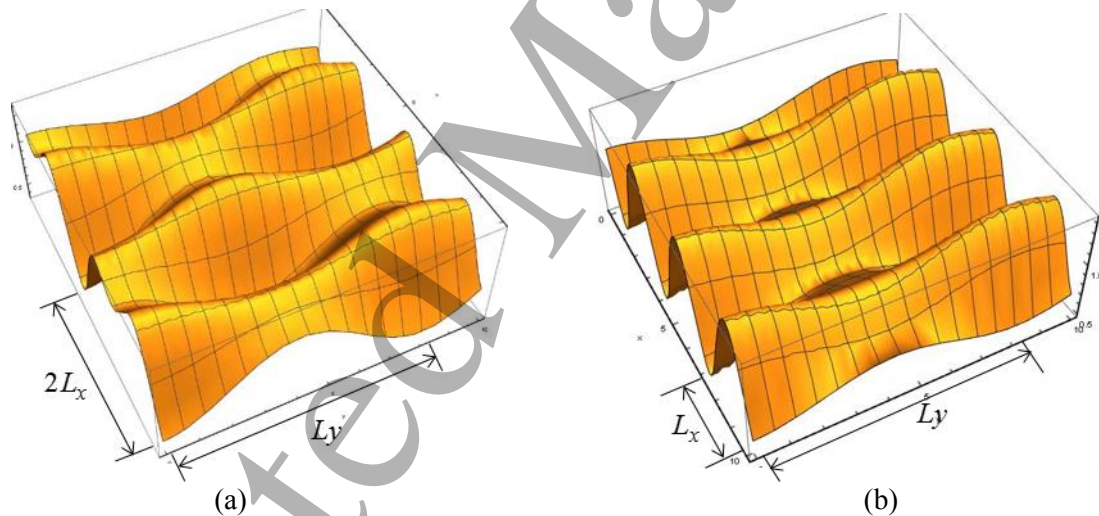

(a)   (b)

Figure 20. Numerical simulation of instability. (a) Staggered pattern mode. (b) Peak-valley mode.

4. Discussions and conclusions

In present study, a series of experiments are shown with various experimental conditions of liquids, falling heights, substrate types and their speeds, and process of pre-wetting. Surface waves are observed on a liquid curtain bridged between the slot exit and the upper surface of a substrate and these waves appear only when the surface tension is much greater than the inertial force, i.e. when $We \ll 1$. In order to study these waves theoretically, the flow of the liquid curtain is divided into two zones, namely, falling and impingement zones (or symmetric and asymmetric zones) on the base of which the curtain profile are simulated and analysed.

The summary and conclusions of the study are as follows:

25

(i) The surface waves appearing on the liquid curtain are varicose waves, which appear due to the pressure difference between inner and outer regions of the meniscus on the substrate. They propagate upstream and become stationary because of the downstream flow.

(ii) The wave number of the surface waves depends on the Weber number and the Reynolds number, while the decay rate of amplitude is more influenced by the Capillary number. They are influenced by the experimental conditions, such as liquids, falling heights, substrate speed, and the process of pre-wetting.

(iii) Even with the same boundary conditions, there are multiple solutions for the curtain profile. The number of solutions depends on the slope and curvature of the curtain surface at the lower boundary, which may be related to the meniscus angle and the pressure inside of the meniscus. Nevertheless, in our experiments, only one solution was actually observed and relevant to interpreting the experiments while the other two solutions were rejected on physical grounds.

(iv) Two types of modes for the instability of the surface waves, i.e. staggered and peak-valley patterns, depend on the Reynolds number, the Weber number, and the amplitude of these waves. The mode of staggered pattern is observed in the experiment while the mode of peak-valley pattern is not. Compared with the mode of staggered pattern, the appearance of the peak-valley pattern requires a much greater amplitude of the waves, a much higher Weber number and Reynolds number.

(v) Curtain coating with a low-Weber-number liquid flow, i.e. $We \ll 1$, can be applied in engineering on the condition of a small falling height, a low substrate speed, and liquids with high viscosity and low surface tension, in which case the surface waves do not appear.

References
[1]   S J Weinstein and K J Ruschak 2004 Coating flows *Annu. Rev. Fluid Mech.*, **36** 29-53
[2]   S F Kistler and P M Schweizer 1997 *Liquid Film Coating* Schweizer London Chapman & Hall
[3]   Yekun Liu, M Itoh, H Kyotoh and K Nakano 2015 *Coating onto a prewet substrate with low Weber number liquid curtain* Seoul ASME-JSME-KSME Joint Fluids Engineering *Conf* **1A** Symposia Part 2
[4]   S P Lin 2003 *Break up of Liquid Sheets and Jets* New York Cambridge University Press
[5]   H Kyotoh, K Fujita, K Nakano and T Tsuda 2014 Flow of a falling liquid curtain into a pool *J. Fluid Mech.* **741** 350-376
[6]   P J Schmid and D S Henningson 2002 On the stability of a falling liquid curtain *J. Fluid Mech.* **463** 163-171
[7]   D S Finnicum, S J Weinstein and Kenneth J. Ruschak 1993 The effect of applied pressure on the shape of a two-dimensional curtain falling under the influence of gravity *J. Fluid Mech.* **255** 647-665
[8]   T D Blake, A Clarke and K J Ruschak 1994 Hydrodynamic Assist of Dynamic Wetting *AIChE Journal* **40** 229-242
[9]   T D Blake 2006 The physics of moving wetting lines *J. Colloid Interface Sci.* **299** 1-13
[10]   T D Blake, R A Dobson and K J Ruschak 2004 Wetting at high capillary numbers *J Colloid and Interface Science* **279** 198-205
[11]   J O Marston and M J H Simmons 2006 Influence of the flow field in curtain coating onto a prewet substrate *Physics of Fluids* **18**, 112102

[12]   E Vandre, M S Carvalho and S Kumar 2014 Characteristics of air entrainment during dynamic wetting failure along a planar substrate *J. Fluid Mech.* **747** 119-140

[13]   G Coppola, F D Rosa and L D Luca 2013 Surface tension effects on the motion of a free-falling liquid sheet *Physics of Fluids* **25**, 062103

[14]   S P Lin 1981 Stability of a viscous liquid curtain *J. Fluid Mech.* **104** 111-118

[15]   X Li and R S Tankin 1991 On the temporal instability of a two-dimensional viscous liquid sheet *J. Fluid Mech.* **226** 425-443

[16]   X Li 1993 Spatial instability of plane liquid sheets *Chem. Eng. Sci* **48** 2973-2981

[17]   E S Benilov, R Barros and S B G O Brien 2016 Stability of thin liquid curtains *Physical Review* **E94** 043110

[18]   L J Liu, L J Yang and H Y Ye 2016 Weakly nonlinear varicose-mode instability of planar liquid sheets *Physics of Fluids* **28**, 034105

[19]   S F Kistler 1984 *The Fluid Mechanics of Curtain Coating and Related Viscous Free Surface Flows with Contact Lines* Ph.D. thesis The University of Minnesota

[20]   S F Kistler and L E Scriven 1994 The Teapot Effect: Sheet-forming Flows with Deflection, wetting and hysteresis *J. Fluid Mech.* **263** 19-62

[21]   N Le Grand-piteria, P Brunet, L Lebon, and L Limat 2006 Propagating wave pattern on a falling liquid curtain *Physical Review* **E74** 026305

[22]   Jean-Marc Chomaz 2001 The dynamics of a viscous soap film with soluble surfactant *J. Fluid Mech.* **442** 387-409

[23]   T Herbert 1983 Secondary instability of plane channel flow to subharmonic three-dimensional disturbance *Physics of Fluids* **26**, 871-874

[24]   W Magnus and S Winkler 1979 *Hill's equation* New York Dover Phoenix Editions